Platen Parallelism Significance and Control in Single Fiber Transverse Compression Tests

Jason Govilas[a], Violaine Guicheret-Retel[a], Fabien Amiot[a], Johnny Beaugrand[b], Vincent Placet[a], Cédric Clévy[a]

[a] FEMTO-ST Institute, UMR 6174, Univ. Bourgogne Franche-Comté, UFC/CNRS/ENSMM/UTBM, 25000 Besançon, France

[b] INRAE, UR 1268 BIA Biopolymères Interactions Assemblages, 44316 Nantes, France

Abstract

Transverse compression tests are the established way to identify the transverse mechanical properties of single fibers. However, to the authors knowledge, the influence of an angle between the two compression platens has never been studied or quantified. In this paper, the importance of platen parallelism is studied for the first time through: numerical simulation and experimental investigation. A sensitivity analysis complements these studies by highlighting the importance of contact geometry in the analytical model, used in the inverse identification of the fiber's apparent transverse elastic modulus E_T. Experimental results show that a misalignment of 1° between the platens produces a variation of more than 35% on the identified E_T, compared to a compression with parallel platens. Given the importance of platen misalignment angle an experimental setup and protocol are designed in order to maintain this angle below 0.1°, thus keeping the error on E_T below 5%.

Keywords: A. Fiber; C. Analytical modelling; C. Finite element analysis; D. Mechanical testing.

1. Introduction

Both synthetic and natural fibers are extensively used in a variety of materials, notably in the textile and composite material industries. Considering the wide range of applications of these materials, transverse loads, perpendicular to the main fiber axis, are common during their entire lifecycle. Ballistic impacts represent a typical example where withstanding these transverse loads is critical [1]. Important transverse loads can also occur during processing and fabrication steps, such as plant fiber extraction and separation [2] or during composite compression molding [3]. Therefore, in order to better model and understand the behavior of fiber-containing materials, but also to ensure fiber integrity during processing

steps, a precise knowledge of fiber transverse properties is crucial. Single Fiber Transverse Compression Tests (SFTCTs) allow a direct undertaking of this task. However, the small size of individual fibers (diameter between 1µm and 100µm), means that high precision measurements are necessary, in addition to specialized equipment to manipulate and observe them. The first tests were performed in the 1960s and 1970s on polymer [4][5][6] and Kevlar fibers [7], quantifying their transverse properties for the first time. Analytical models of the test, based on Hertzian contact theory were also developed in these works. Kawabata et al. [8] created the first mechatronic setup for fiber transverse compression in the 1990s, significantly improving measurement accuracy, thus renewing the interest for SFTCTs. Many transverse compression experiments, performed on various synthetic fibers (carbon, Kevlar, polymer), iterated on Kawabata's setup, gradually improving measurement quality [9][10]. Finite element analysis was also used in parallel to such experimental studies [11][12][13][14].

While the testing methods and tools have evolved over the years, the basic principle of the test remains unchanged. A single fiber is compressed between a fixed and a mobile platen, with the applied compressive force and displacement of the mobile platen being the most popular measured quantities. Analytical models are then used to identify the apparent transverse elastic modulus E_T by inverse method. They are all based on Hertzian contact between a right circular cylinder and a half-space, as a means of considering the change in the contact geometry during the fiber's transverse compression. Consequently, a common characteristic of these models is their sensitivity to the fiber-platen contact surface. Fiber geometry and roughness can influence this contact surface; however, they can be difficult to control, especially in the case of plant fibers where, elliptical cross-sections, twists around the main axis and coarse surfaces are common. While knowledge on the influence of elliptical geometries is poor it can significantly impact contact surface. When it comes to roughness however, the impact of contact friction between fiber and platens on the fiber's stress-strain response has been shown to be minimal through finite element analysis [15]. On the other hand, platen geometry is easier to control, limiting its influence on contact surface. Choosing appropriate materials (metals, sapphire, glass), characterized by a low roughness and high stiffness leads to smooth and regular geometries.

In addition to fiber and platen geometry and roughness, platen parallelism can have a major influence on contact surface. Its influence is not limited to SFTCTs but has also been recognized in the field of compression in general. The "Brazilian test", an indirect method to measure tensile strength of samples

through compression in civil engineering and rock mechanics is one of the most notable examples [16][17][18]. A standardization of the test proposed in 1978 suggested that compression jaws need to be "parallel within 0.25°" [19], without quantifying however the induced error. Other compression studies report platen parallelism as well. In his review on uniaxial compression, B. W. Darvell notes that platen parallelism is "essential" though "rarely commented on in the print" [20]. In their study of strain rosettes under compression, E. Little et al. also identified platen parallelism as "the most predominant of the factors investigated" [21]. When it comes to SFTCTs, all analytical models rely on a perfectly parallel compression platen hypothesis. Only few authors however consider platen misalignment and propose means to experimentally adjust platen parallelism. Yet, descriptions are usually extremely short and can even lack any sort of methodology, hindering reproducibility. Hadley et al. [4] manually adjust parallelism using a screw mechanism, Jones et al. [22] propose an apparatus with an aligning sphere, while Wolbrett-Blitz et al. [13] use three external stepping motors. Sockalingam et al. [14] and Naito et al. [23] propose methods using platen preloading. A unique approach is proposed by Guo et al. [24] who propose a simultaneous compression of two fibers to avoid a rotation of the upper platen around the main fiber axis. Ultimately, even though platen parallelism is recognized as an important parameter and could explain variations in measured transverse properties, no clear and widely adopted solution exists to control it. Furthermore, to the authors knowledge, no direct quantification of the angle between the two compression platens has ever been performed and its influence on measured material properties has never been studied.

Fig. 1 illustrates a compression platen misalignment produced by a rotation along the fiber's longitudinal x axis (angle θ) and a rotation along its horizontal transverse y axis (angle ϕ). In the case of a ϕ angle rotation, only part of the fiber will be compressed. The contact area is thus heavily affected. In contrast, the whole fiber length will still be compressed in the case of a θ angle rotation. Furthermore, the circular cross section of the fiber minimizes the effects of a small θ angles. Taking this into consideration; this paper focuses on the ϕ angle and the term 'tilt angle' will be used to describe it. The tilt angle is unique to the transverse compression of fibers, since their length is significantly larger than their diameter. Compression of more spherical objects such as millimetric silica gravel [25], micrometric cells [26] or sub-micrometer particles [27], are less sensitive to small tilt angles.

To demonstrate and quantify the influence of the tilt angle on SFTCTs, three complementary approaches are proposed: (i) a sensitivity analysis of the analytical model, (ii) a finite element analysis and (iii) an experimental approach using a micro-mechatronic setup. Revealing the role of the tilt angle through three distinct methods, ensures that the experimentally observed phenomena are not due to other omitted parameters. For (ii) and (iii), a SFTCT is performed experimentally or simulated, with different tilt angles. The identified apparent transverse elastic modulus for each angle is compared to a reference modulus, identified from a transverse compression with parallel platens. The tilt's angle influence can consequently be quantified through the variation of E_T. An experimental protocol is also established, to quantify the influence of the tilt angle but also to set it below $0.1°$. The experimental setup aims therefore at a precise and reproducible control of platen parallelism, reducing its effects on material property identification.

2. Materials and methods

2.1. Analytical model and sensitivity analysis

Many fibers are known to exhibit complex material behavior that can deviate from a pure elastic response, due to structural parameters such as skin/core interactions [13][28] or combinations of viscous and plastic material behavior [10][14][28]. While elastic-plastic [11][28] and inelastic [14] behaviors have been studied through finite element analysis, to the authors knowledge no unified analytical model has been developed to describe such behaviors. Existing analytical models of SFTCTs, consider the fiber as a transversely isotropic elastic material. With such models, a fiber's behavior is thus studied through its apparent elastic parameters while omitting structural or material generated inelasticity.

The model developed by Abdul Jawad and Ward [6] is used for this purpose. It models a single fiber in transverse compression as a right circular cylinder in plane strain conditions, between two parallel and rigid platens. An infinitesimal strain approach is used. A Hertzian contact between fiber and platens is considered, taking into consideration the change in contact geometry during compression. The model is expressed as follows:

$$U = -\frac{4F}{\pi}\left(\left(S_{11} - \frac{S_{13}^2}{S_{33}}\right)\right)\left(\operatorname{arcsinh}\left(\frac{R}{b}\right) + 0.69\right) + \frac{2F}{\pi}\left(S_{11} + S_{12} - \frac{2S_{13}^2}{S_{33}}\right) - \frac{4F}{\pi}\left(\left(S_{12} - \frac{S_{13}^2}{S_{33}}\right)\left(\frac{R}{b}\right)\left(\sqrt{1 + \left(\frac{R}{b}\right)^2} - \frac{R}{b}\right)\right) \quad (8)$$

with U : the transverse contraction of the cylinder, F: the applied compressive force normalized by the contact length (N/m), R: the radius of the fiber. S_{ii} represent the coefficients of the fiber's compliance matrix:

$$S_{11} = \frac{1}{E_T};\ S_{12} = -\frac{\nu_{TT}}{E_T};\ S_{13} = -\frac{\nu_{TL}}{E_T}; S_{33} = \frac{1}{E_L} \quad (9)$$

with: E_L : the longitudinal modulus, E_T: the transverse modulus, ν_{LT}: the major Poisson's ratio and ν_{TT}: the minor Poisson's ratio.

The parameter b is derived from the Hertz solution and represents the contact halfwidth:

$$b = \sqrt{\frac{4FR}{\pi}\left(\left(s_{11} - \frac{s_{13}^2}{s_{33}}\right)\right)} \quad (10)$$

Inverse identification through least square regression analysis can then be performed to identify an apparent transverse elastic modulus E_T. Force F and contraction U measurements are needed as an input along with values for the fiber's geometric and material parameters R, E_L, $\nu_{LT}$and ν_{TT}. To evaluate the influence of these parameters that are not directly measured during SFTCTs, on the apparent transverse elastic modulus E_T, a sensitivity analysis is performed using a variance-based sensitivity analysis (Sobol indices) [29]. A ranking of these parameters can thus be established from most to least influent. An in-house software developed for uncertainty and sensitivity analysis is used. A variation of 10% is allowed for all parameters with nominal values of $E_L, R, \nu_{LT}, \nu_{TT}$ corresponding to the properties of an experimentally tested PA11 fiber being given in *Table 1*. By setting the same variation for all parameters the determined sensitivity of E_T is inherent to the analytical model. A value for the force and displacement are taken from the finite simulation that will be presented in section 2.5.

2.2. Fiber material

A polyamide 11 (PA11) fiber was chosen for experimental testing due to its cylindrical geometry, homogenous structure and transversely isotropic nature, which matches the assumptions made by Jawad's model. Its geometric regularity also limits the influence of the fiber geometry on the fiber-platen contact

surface, ensuring that the tilt angle is the most influential parameter. The fiber's mean diameter was measured as $D = 35.1 \pm 0.3\ \mu m$ (mean value and standard deviation) along 6 cross sections along the fiber length, using the Fiber Dimensional Analysis System (FDAS770) from DIA-STRON. Placet et al. [30] measured the properties of this fiber lot at a nominal value of $E_L = 2155\ MPa$, for the longitudinal elastic modulus and $\nu_{TT} = 0.07$, for the minor Poisson's ratio. The major Poisson's ratio is set at $\nu_{LT} = 0.4$, based on data from the bulk material provider. These are the geometric and material properties that were considered for the PA11 fiber throughout the experimental and numerical studies but also as the nominal values in the sensitivity analysis. Their values and source are summarized in *Table 1*.

2.3. Experimental setup

The experimental setup used to perform SFTCTs is an upgraded version of the micro-mechatronic setup presented by Placet et al. [30]. *Fig. 2* presents the setup from different angles to display all of its components. A single fiber is placed on a fixed anodized aluminum lower platen, with a roughness measured at $S_a = 0.98 \mu m$ (mean arithmetic surface height). Two microscopes offer an observation of the fiber length and its cross section. A dedicated force-displacement sensor is placed above the fiber. The sensor gets directly in contact with the fiber in order to compress it, thus replacing conventional mobile platens [4][14]. It is capable of measuring up to $350\ mN$ with a precision of $0.1\ mN$ in force and $30\ nm$ in displacement, allowing the detection of subtle changes in fiber behavior. In order to control its tilt angle, the sensor is mounted on a rotary actuator (*SmarAct SR-2013*) offering a 25 µ° resolution. To move the sensor towards the fiber and compress it, the sensor- rotary actuator assembly is mounted on a linear piezoelectric nanopositioner (*PI PIHera 629.1*) with a resolution of 14 nm.

The sensor's design can be seen on *Fig. 3*. It is a compliant structure designed with high off axis stiffness through a compliant translational joint (CT-joint) architecture [31]. Off-axis movements are thus greatly limited, allowing sensor deformation only in the measurement axis, which contributes to a linear sensor response. It is a product of clean room fabrication on a 500µm thick, silicon wafer. Being a brittle material [32], silicon will present no plastic behavior and exhibit a linear elastic behavior. The sensor is composed of 3 main parts: *(i)* the upper part, connected to the linear actuator; *(ii)* the lower part, whose tip gets directly in contact with the fiber; *(iii)* a series of beams connecting the upper and lower parts. Fiducial markers, similar to QR codes, are printed by photolithography on the upper and lower parts, at the center of the sensor. The vertical coordinate of each marker can be measured with the help of a

microscope that faces them directly [33]. The horizontal position and in plane rotation can also be measured. The views obtained by the three different microscopes can be seen on *Fig. 4*.

The sensor's operating principle can be summarized as follows: the linear actuator moves the sensor downwards, establishing a direct contact between its lower part and the fiber. Once the contact is established, a compressive load is generated and the sensor's beams start bending. This allows the upper part of the sensor to continue its downwards movement. The lower part however, moves only as much as the fiber contracts. A relative displacement ΔY is hence generated between the two parts of the sensor. It can be obtained through the measured vertical coordinates of the fiducial markers with:

$$\Delta Y = Y_u - Y_l \quad (1)$$

where: Y_u is the vertical coordinate of the fiducial marker on the sensor's upper part and Y_l the one on its lower part. Consequently, the applied compressive force can be calculated by:

$$F = k \cdot \Delta Y \quad (2)$$

with k being the sensor's stiffness. The sensor is calibrated by compressing a reference force sensor (*TEI FSB 101*). The signal from the reference force sensor and the relative displacement ΔY give access to the sensor's stiffness through linear regression. It is measured at $k = 619{,}4 \pm 0.9 \frac{N}{m}$ (mean value and standard deviation) across 10 repeated loading-unloading compression cycles. Great linear correlation between force and displacement data is shown with an average Pearson correlation coefficient [34][35] of $\rho = 0.99$, where a value of 1 represents a perfect correlation. The displacement of the sensor's lower part corresponds directly to the fiber's contraction U, as soon as the contact is established. It can thus be calculated by:

$$U = Y_l - Y_{lc} \quad (3)$$

where Y_l is the current vertical coordinate of the lower fiducial marker and Y_{lc} its coordinate when the contact is first established (where Y_u first becomes greater than Y_l). Contrary to most experimental setups used in SFTCs, the measurement of the fiber contraction is performed very close to the sample. Errors in displacement measurements related to system compliance are hence avoided.

2.4. Experimental platen parallelism control

To ensure good platen parallelism during SFTCTs, an experimental protocol is necessary to minimize the tilt angle. A methodology is developed, based on the evolution of the distance between two objects,

when one of them is subject to a rotation. In the present case, the objects are the fixed platen and the force-displacement sensor, rotating with an angle α given by the rotary actuator. The sensor is modeled as a rectangle of length L and width w, with a distance of Y_0 from the fixed platen when the tip of the sensor is parallel to the fixed platen. The length L is the distance between the sensor's tip and the rotation center of the rotary actuator. A representation of the sensor-fixed platen configuration for an angle $\alpha > 0$, is given in *Fig. 5.* In this case, if the sensor moves downwards, the point 1 is the first to get in contact after moving by:

$$Y_c = Y_0 + L(1 - \cos(\alpha)) - \frac{w}{2}\sin(\alpha) \quad (4)$$

If $\alpha < 0$, the point 2 is the first one to get in contact with the platen after moving by:

$$Y_c = Y_0 + L(1 - \cos(\alpha)) + \frac{w}{2}\sin(\alpha) \quad (5)$$

In general, the distance between sensor tip and fixed platen can be written as:

$$Y_c = \begin{cases} Y_0 + L(1 - \cos(\alpha)) - \frac{w}{2}\sin(\alpha), & if\ \alpha \geq 0 \\ Y_0 + L(1 - \cos(\alpha)) + \frac{w}{2}\sin(\alpha), & if\ \alpha < 0 \end{cases} \quad (6)$$

Fig. 6. shows the distance Yc as a function of the angle α. Its overall shape is similar to a lower-case omega (ω) with the parallelism between sensor and platen located at the center tip.

In practice, different misalignments with respect to the vertical axis occur during the assembly of the different components (sensor, rotary actuator, nanopositioner). Therefore, the reference position of the rotary actuator ($\alpha = 0°$) does not correspond to a sensor parallel to the lower platen. An angle β is thus introduced to describe the combination of all these misalignments. Consequently, the rotary actuator has to generate a rotation of $\alpha = -\beta$ from its reference position, to ensure parallelism. In order for β to represent all misalignments between the sensor and nanopositionner, L now represents the distance between the sensor's tip and an apparent rotation center point located on the nanopositioner instead of the rotary actuator. The new equation can be written as follows:

$$Y_c = \begin{cases} Y_0 + L(1 - \cos(\alpha + \beta)) - \frac{w}{2}\sin(\alpha + \beta), & if\ \alpha \geq 0 \\ Y_0 + L(1 - \cos(\alpha + \beta)) + \frac{w}{2}\sin(\alpha + \beta), & if\ \alpha < 0 \end{cases} \quad (7)$$

Using this analytical model, the necessary rotation generated by the rotary actuator that ensures a sensor-fixed platen parallelism can be determined experimentally. The sensor is lowered and pressed against the fixed platen for different α angles. Using a manual positioning stage, the same contact zone is kept to minimize the influence of the fixed platen geometry. The distance Y_c corresponds to the distance

travelled by the sensor's lower part, Y_l, until it gets in contact with the rigid support and stops moving. Y_c is consequently measured for a large number of α values in the range of -3° to 3°. Equation (7) is then used to fit the experimental $Y_c(\alpha)$ points using a least-squares algorithm, thus giving the value of the misalignment angle β. This process was repeated 4 different times on the same zone of the fixed compression platen.

The sensor's tip width w is equal to $300\ \mu m$. The value of Y_0 and β are left as unknown parameters in the inverse identification. Since the apparent center of rotation on the nanopositioner cannot be defined accurately, the parameter L is also considered as an unknown.

2.5. Finite element modeling

In addition to the experimental SFTCTs, a simulation of the test is performed with various tilt angles, thus offering another tool to study the influence of platen parallelism. A finite element model was created using COMSOL Multiphysics® to simulate the transverse compression test. The geometry, boundary conditions and mesh of the model can be seen on *Fig. 7*. The details of the model are given below.

In order to account for the presence of a tilt angle on the upper compression platen, a 3D model is necessary. The fiber is modelled as a right circular cylinder of a transversely isotropic material. Its transverse elastic modulus E_T is equal to the experimentally measured PA11 modulus. The cylinder is positioned between two rectangular platens. The material chosen for the platens is significantly stiffer than the cylinder, isotropic and elastic. The length of both the fiber and platens is set as equal to the width of the sensor's tip that is used in experiments. Geometric and material parameter values for the fiber and the platens are given in *Table I* and *Table II* respectively. To better approximate Jawad's model infinitesimal strain approach, linear strain formulation is used in the model.

Contact pairs between the platen and the cylinder are defined, using an augmented Lagrangian formulation. The platens being stiffer, are chosen as the masters in the contact pairs with the cylinder being the slave. To simulate the transverse compression test, the lower platen's movement is completely blocked ($\{u\} = 0$) while the upper platen is moved by 1µm along the vertical z axis with its off-axis movements being blocked ($u_x = 0, u_y = 0, u_z = -1\mu m$). The tilt angle is created by rotating the upper platen around the y axis.

Even though modeling the problem in 3D is necessary, reducing its size and complexity is possible. A geometric symmetry is present along the xz plane, therefore only half of the cylinder and platens need to be modelled if a symmetry condition $\{u\} \cdot \vec{y} = 0$, is applied along the xz plane. To reduce computation time, a potential contact between platen and cylinder is searched on an area with a width of $D/5$ where D is the diameter of the cylinder. The contact width never exceeds this zone during simulations.

When it comes to meshing, being the slave of the contact pair, the cylinder is meshed much more finely than the platens. Special attention is given to the contact surface, with 12 mesh elements along the defined contact zone. When there is a tilt angle, the number of elements along the cylinder's length is more important close to the contact zone, following an exponential distribution. The number of elements in the vertical direction is also larger close to the contact zones. This locally refined mesh ensures that the zones close to the cylinder-platen contact, where the stress gradients are the largest, are modelled with a higher precision, while the zones far from the compression are meshed more coarsely. Further computation time is therefore saved while maintaining accurate results.

2.6. Tilt influence study

Quantifying the influence of the tilt angle on the identified transverse elastic modulus is achieved via the same method for both the experimental and numerical studies. A first test is performed or simulated between parallel platens. In the case of the experimental study this means that the identified misalignment angle is corrected through a rotation of the rotary actuator. Once the compression is done the compressive force per unit of length F and fiber contraction data U are provided to Jawad's model, along with nominal values for E_L, ν_{LT}, ν_{TT} and R. An apparent transverse elastic modulus E_{T0} is then identified with a least square, trust region algorithm and serves as a reference hereafter. An average residual of the least square regression r is calculated with:

$$r = \frac{1}{N}\sqrt{\sum_{i=1}^{N}\left(U_i - U_{i_{model}}\right)^2} \quad (11)$$

with: N the number of data points, U_i the experimental or simulated displacement data and $U_{i_{model}}$ the displacement predicted by Jawad's model.

In the case of the experiments, the force and contraction data are measured by the force-displacement sensor as described in section 2.2. In the case of the simulation the fiber contraction corresponds directly to the vertical displacement imposed to the mobile platen. The force is obtained through a surface integration of the contact pressure between the mobile platen and the fiber. Since the analytical model does not take the tilt angle into consideration the contact length, it is considered to always be equal to the fiber length. Both experimental and simulation force data are thus divided by the fiber length, to obtain a force per unit of fiber length

Tests or simulations are performed with tilt angles varying from -1° to 1° in the case of the experimental studies and from 0° to 1° for the simulations, with increments of 0.1° between tests. An elastic modulus E_{Ti} is identified for each angle. To quantify the influence of the tilt angle, the relative deviation from E_{T0}, ΔE_T, is calculated for each E_{Ti} :

$$\Delta E_T = \frac{E_{Ti} - E_{T0}}{E_{T0}} \quad (12)$$

In the case of the experimental studies a few extra steps must be taken to guarantee the validity of the tests. To ensure that the fiber's behavior is repeatable and differences in identified properties are induced by the tilt angle, the fiber was loaded 10 consecutive times, with a minimized tilt angle, before performing the tilt influence study. Therefore, an independence of the fiber's apparent transverse elastic modulus from its loading history can be demonstrated at the chosen displacement amplitude. Changes in E_T when the compression is done with a tilt angle can consequently be attributed to the loss of parallelism while plastic deformation and time dependent viscous behavior can be omitted.

For each tilt angle the fiber goes through a single loading and unloading cycle. During the loading phase the fiber exhibits some rigid body motions and small rotations before being completely confined between the sensor's tip and the fixed plated where it starts compressing. For this reason, apparent transverse elastic moduli were identified on the unloading phase where the fiber's rigid body motions are less significant. For the entire testing procedure, the sensor was moved downwards at $10\mu m/s$ with the same generated displacement from the nanopositioner. Once the maximum compression amplitude was reached it was maintained for a total of 5s before starting the unloading phase.

3. Results and discussions

3.1. Sensitivity analysis study

The total Sobol index for each model parameter is given in *Fig. 8*. The Sobol index for the fiber radius R is significantly higher when compared to the other variables. Therefore, a variation of the fiber radius causes the largest variation of E_T. The fiber radius is the sole geometric parameter in Jawad's model. With E_T being so sensitive to this parameter, the importance of geometry and by consequence, the importance of the contact surface during transverse compression tests is highlighted. Since the contact surface is strongly related to the tilt angle between compression platens, this sensitivity analysis strongly points, even though indirectly, to the key role of the tilt angle during SFTCTs.

3.2. Finite element analysis study

Fig.9 shows the evolution of the contact force as a function of the mobile platen displacement for three different simulated tilt angles. The fitted analytical model can be seen along with the evolution of the average residual r. For parallel plates the analytical model follows the simulation data closely, resulting in a low value of r. With the increase of the tilt angle and resulting decrease in contact surface, the contact force decreases for a given upper platen displacement. The non-linearity of the force displacement curves also changes. The analytical model cannot match this behavior as closely leading in a worse fit, as can be seen in the values of the residual r.

These changes are reflected on the identified transverse elastic modulus E_T. *Fig. 10* shows the relative variation ΔE_T as a function of the tilt angle. Its influence is major, with an angle of 1° causing a decrease of 92% on the identified E_T. This decrease is related with the decrease in contact surface in the presence of a tilt angle. The subsequent contact force decreases for a given upper platen displacement, which results in a lower slope. Thus, E_T gets underestimated with the increase in tilt angle, decreasing rapidly for smaller angles and decelerating towards tilts of 1°. SFTCTs simulations, therefore directly demonstrate the key role of the mobile platen's tilt angle.

While fitting quality is good when the tilt angle is equal to zero, a difference of 3.8% exists between the transverse elastic modulus defined in the finite element model and the modulus identified by Jawad's analytical model through force-displacement simulation data. Different sources can explain this difference. The analytical model is formulated in plane strain conditions, no longitudinal strain is thus

considered. In the case of the 3D finite element model longitudinal strains will be present, especially closer to the fiber edge. Especially for fibers such as PA11 where the anisotropy ratio E_L/E_T is quite low, longitudinal strains become more important and the differences with the analytical model become more apparent when compared to fibers with a high anisotropy ratio ($E_L/E_T > 10$). Some deviation can also be attributed to differences between Hertz's analytical description of the contact and its finite element modeling through an augmented Lagrangian formulation. Despite these differences between the finite element and analytical model the variations induced by the tilt angle are much larger and can only be explained by a high sensitivity of the E_T identification to platen parallelism.

3.3. Experimental study

3.3.1. Tilt angle minimization

An example of the distance travelled by the force-displacement sensor to get in contact with the fixed platen, as function of the angle α, given by the rotary actuator, is given in *Fig. 11*. An apparent "omega tip" corresponding to a parallel sensor tip and fixed platen can be seen on the experimental data at 0.57°. The analytical model is fitted to the experimental data using a least-squares, trust region algorithm. A good correlation is observed between the experimental results and the model. Across 4 different tests, the misalignment angle is identified at $\beta = -0.58° \pm 0.01°$. This means that the actuator has to rotate at an angle of $\alpha = +0.58°$ from its reference position in order to minimize the tilt angle and make the sensor tip parallel to the fixed platen. At this identified position, the tilt angle between the sensor tip and fixed platen is considered as $\phi = 0°$. The distance L is identified at $L = 70 \pm 0.8$ mm (mean value and standard deviation), which corresponds to a distance between the sensor tip and a point on the nanopositioner, situated across 2/3 its length. The good fitting of the model, small standard deviation of L along with its value that corresponds to a realistic sensor-nanopositioner distance, altogether validate the approximation that was selected to represent the inherent misalignments in the experimental setup. Taking all this into consideration the proposed experimental protocol ensures a sensor-platen parallelism with an accuracy below 0.1°.

3.3.2. Experimental tilt influence

After 10 consecutive loading-unloading cycles at the identified minimized tilt angle configuration, the apparent transverse elastic modulus of the PA11 fiber, identified from the unloading phase, is $E_T =$

$706. \pm 32 MPa$ (mean value and standard deviation). The standard deviation represents a variation of 4.45% of the mean value. The identification of the apparent elastic modulus is thus repeatable, the fiber's inelastic behavior can thus be safely omitted from the study of the tilt angle's influence.

For tests on the PA11 fiber with a varying tilt angle, its influence can already be seen on the force-displacement data. *Fig. 12* shows the compressive force as a function of fiber contraction for three distinct values of the tilt angle. The fitted analytical model can also be seen along with the evolution of the average residual r The fiber behavior is noticeably different between tests with a parallel sensor-platen configuration and a tilt angle of 1°. Tilt angles lead to a smaller contact area than with parallel plates, resulting in a decrease in contact force for a given displacement, just as shown by the finite element analysis. However, contrary to the simulations no clear trend can be observed in the evolution of the average residual r. This is related to the sensor's precision in displacement measurement of $30nm$. This means that residues of $5\ nm$, as seen in the simulation of transverse compression with parallel plates are not attainable. However, $r$values remain low attesting to a good fitting quality. The identified elastic modulus for a tilt angle that is equal to zero, E_{T0}, is $685.7\ MPa$ which is within the standard deviation range of previously identified elastic modulus.

The impact of tilt angles can also be seen on the fiber's identified elastic parameter. *Fig. 13* shows the variation of the identified transverse elastic modulus ΔE_T as a function of the tilt angle. An angle of 1° causes a decrease in the identified E_T of up to 35%. This is much higher than the variation of 4,45% observed during repeated tests with a minimized tilt. The large variations of E_T in the tilt study can consequently be attributed to the tilt angle.

When comparing the evolution of ΔE_T between the finite element and experimental studies the influence of the tilt angle seems overestimated in the simulations. This difference can be attributed, at least partially, to sensor torsion. During experiments in a non-parallel configuration, the sensor's torsion can compensate to some extent part of the tilt angle. This realignment cannot occur in simulations where the mobile platen is moved along the vertical axis, with no permitted off-axis movements, resulting in a higher influence of the tilt angle. Another difference between the two studies is the evolution of ΔE_T as a function of the tilt angle. The highly controlled and well-defined finite element model leads to a smoother decrease. The same cannot be said for the experiments were more irregularities are present. They can also

be attributed to some extent to sensor torsion, but mainly to measurement noise, variations in fiber and fixed platen geometry or sliding motions of the fiber between sensor tip and fixed platen.

4. Conclusions

Single fibers are a challenging material to test which can often lead to important dispersion in experimentally measured data. A precise control of the most influent parameters is thus crucial. In the case of SFTCTs the tilt angle is shown to be such a parameter. Its influence on the transverse elastic modulus E_T, as identified by SFTCTs, is demonstrated and quantified for the first time through three different methods:

a. A global sensitivity analysis reveals the sensitivity of E_T to the fiber radius, sole geometric parameter in the analytical model, demonstrating the importance of the platen-fiber contact surface and thus showing indirectly the importance of the tilt angle.
b. A finite element model to simulate fiber transverse compression tests under varying tilt angles. The influence of platen parallelism is directly shown, with a tilt of 1° generating a 92% decrease on the identified value of E_T.
c. An experimental study on a PA11 fiber, employing a specialized micro-mechatronic setup. The fiber's apparent E_T at the unloading phase, decreases by 35% for a tilt angle of 1°, thereby demonstrating in practice the key role of the tilt angle.

This work establishes that the tilt angle needs to be controlled precisely during single fiber transverse compression tests in order to limit the resulting measurement errors on the apparent transverse elastic modulus. For this reason, an experimental protocol is also presented, that enables a precise control of the tilt angle, minimizing it with a precision below 0.1°. With this precise control, fiber behavior better matches analytical predictions and allows the measurement of transverse elastic properties with higher accuracy.

Even though these studies were performed in the case of fiber transverse compression, it is safe to assume that similar results regarding the influence of the tilt angle could be obtained in the case of different objects subject to uniaxial compression. The proposed experimental setup, coupled with its parallelism setting protocol could be used to compress such fiber-scale sized samples or even sub-

micrometric objects while ensuring a high degree of precision, whereas the parallelism setting protocol could be the basis for tilt angle control for compression at any scale.

Acknowledgements

These works have been supported by the European Union's Horizon 2020 research and innovation program under grant agreement No 771134. The project NETFIB was carried out under the ERA-NET Cofund SusCrop (Grant N°771134), being part of the Joint Programming Initiative on Agriculture, Food Security and Climate Change (FACCE-JPI). This work has also been supported by EIPHI Graduate School under (“ANR-17-EURE-0002”), the French RENATECH network through its FEMTO-ST technological facilities MIMENTO as well as the Robotex network ("ANR-10-EQPX-44-01"). Authors acknowledge Joel Agnus, Guillaume Laurent, Antoine Andre, Patrick Rougeot, Melissa Blot, Frédérique Trivaudey and Anouk Chevallier for their help and support.

[1] Abtew MA, Boussu F, Bruniaux P, Loghin C, Cristian I. Ballistic impact mechanisms – A review on textiles and fibre-reinforced composites impact responses. Compos Struct 2019;223:110966. https://doi.org/10.1016/j.compstruct.2019.110966.

[2] Bourmaud A, Beaugrand J, Shah DU, Placet V, Baley C. Towards the design of high-performance plant fibre composites. Prog Mater Sci 2018;97:347–408. https://doi.org/10.1016/j.pmatsci.2018.05.005.

[3] Comas-Cardona S, Le Grognec P, Binetruy C, Krawczak P. Unidirectional compression of fibre reinforcements. Part 1: A non-linear elastic-plastic behaviour. Compos Sci Technol 2007;67:507–14. https://doi.org/10.1016/j.compscitech.2006.08.017.

[4] Hadley D., Ward I., Ward J. The transverse compression of anisotropic fibre monofilaments. Proc R Soc London Ser A Math Phys Sci 1965;285:275–86. https://doi.org/10.1098/rspa.1965.0103.

[5] Morris S. 39—The Determination of the Lateral-Compression Modulus of Fibres. J Text Inst 1968;59:536–47. https://doi.org/10.1080/00405006808660016.

[6] Jawad SA, Ward IM. The transverse compression of oriented nylon and polyethylene extrudates. J Mater Sci 1978;13:1381–7. https://doi.org/10.1007/BF00553190.

[7] Phoenix S, Skelton J. Transverse Compressive Moduli and Yield Behavior of Some Orthotropic, High-Modulus Filaments. Text Res J 1974:934–40. https://doi.org/doi:10.1177/004051757404401203.

[8] Kawabata S. Measurement of the transverse mechanical properties of high-performance fibres. J Text Inst 1990;81:432–47. https://doi.org/10.1080/00405009008658721.

[9] Cheng M, Chen W, Weerasooriya T. Experimental investigation of the transverse mechanical properties of a single Kevlar® KM2 fiber. Int J Solids Struct 2004;41:6215–32. https://doi.org/10.1016/j.ijsolstr.2004.05.016.

[10] Stamoulis G, Wagner-Kocher C, Renner M. Experimental study of the transverse mechanical properties of polyamide 6.6 monofilaments. J Mater Sci 2007;42:4441–50. https://doi.org/10.1007/s10853-006-0655-x.

[11] Kotani T, Sweeney J, Ward IM. The measurement of transverse mechanical properties of polymer fibres. J Mater Sci 1994;29:5551–8. https://doi.org/10.1007/BF00349946.

[12] Singletary J, Davis H, Song Y, Ramasubramanian MK, Knoff W. Transverse compression of

PPTA fibers. Part I. Fiber transverse structure. J Mater Sci 2000;35:583–92. https://doi.org/10.1023/A:1004716108638.

[13] Wollbrett-Blitz J, Joannès S, Bruant R, Le Clerc C, De La Osa MR, Bunsell A, et al. Multiaxial mechanical behavior of aramid fibers and identification of skin/core structure from single fiber transverse compression testing. J Polym Sci Part B Polym Phys 2016;54:374–84. https://doi.org/10.1002/polb.23763.

[14] Sockalingam S, Bremble R, Gillespie JW, Keefe M. Transverse compression behavior of Kevlar KM2 single fiber. Compos Part A Appl Sci Manuf 2016;81:271–81. https://doi.org/10.1016/j.compositesa.2015.11.032.

[15] Sockalingam S, Gillespie JW, Keefe M. On the transverse compression response of Kevlar KM2 using fiber-level finite element model. Int J Solids Struct 2014;51:2504–17. https://doi.org/" ".

[16] Azakawa T. New test method for evaluating internal stress due to compression of concrete (the splitting tension test)(part 1). J Jpn Soc Civ Eng 1943;29:777–87.

[17] Carneiro F. A new method to determine the tensile strength of concrete. Pap Present 5th Meet Brazilian Assoc Tech Rules 1943.

[18] Li D, Wong LNY. The brazilian disc test for rock mechanics applications: Review and new insights. Rock Mech Rock Eng 2013;46:269–87. https://doi.org/10.1007/s00603-012-0257-7.

[19] Bieniawski ZT, Hawkes I. Suggested Methods for Determining Tensile Strength of Rock Materials - 1. Suggested Method for Determining Direct Tensile Strength. Int J Rock Mech Min Sci 1978;15:99–103.

[20] Darvell BW. Uniaxial compression tests and the validity of indirect tensile strength. J Mater Sci 1990;25:757–80. https://doi.org/doi.org/10.1007/BF03372161.

[21] Little EG, Tocher D, Colgan D, O'Donnell P. An analysis of the factors influencing the data derived from a plug type three-dimensional strain rosette under compression and torsion. Strain 2005;41:193–202. https://doi.org/10.1111/j.1475-1305.2005.00230.x.

[22] Jones MCG, Lara-Curzio E, Kopper A, Martin DC. The lateral deformation of cross-linkable PPXTA fibres. J Mater Sci 1997;32:2855–71. https://doi.org/10.1023/A:1018672400459.

[23] Naito K, Tanaka Y, Yang JM. Transverse compressive properties of polyacrylonitrile (PAN)-based and pitch-based single carbon fibers. Carbon N Y 2017;118:168–83.

https://doi.org/10.1016/j.carbon.2017.03.031.

[24] Guo Z, Casem D, Hudspeth M, Nie X, Sun J, Chen W. Transverse compression of two high-performance ballistic fibers. Text Res J 2016;86:502–11. https://doi.org/10.1177/0040517515592814.

[25] Cavarretta I, O'Sullivan C. The mechanics of rigid irregular particles subject to uniaxial compression. Geotechnique 2012;62:681–92. https://doi.org/10.1680/geot.10.P.102.

[26] Chip RM, Sakuma S, Nakahara K, Arai F. Continuous Mechanical Indexing of Single-Cell Spheroids. IEEE Robot Autom Lett 2019;4:2973–80. https://doi.org/10.1109/LRA.2019.2923976.

[27] Yoshida M, Ogiso H, Nakano S, Akedo J. Compression test system for a single submicrometer particle. Rev Sci Instrum 2005;76. https://doi.org/10.1063/1.2038187.

[28] Singletary J, Davis H, Song Y, Ramasubramanian MK, Knoff W. Transverse compression of PPTA fibers. Part II. Fiber transverse structure. J Mater Sci 2000;35:583–92. https://doi.org/10.1023/A:1004716108638.

[29] Sobol IM. Global sensitivity indices for nonlinear mathematical models and their Monte Carlo estimates. Math Comput Simul 2001;55:271–280. https://doi.org/10.1016/S0378-4754(00)00270-6.

[30] Placet V, Blot M, Weemaes T, Bernollin H, Laurent G, Amiot F, et al. Transverse compressive properties of natural fibers determined using micro mechatronic systems and 2D full-field measurements. Mater Today Proc 2020:1–6. https://doi.org/10.1016/j.matpr.2020.01.383.

[31] Trease BP, Moon YM, Kota S. Design of large-displacement compliant joints. J Mech Des Trans ASME 2005;127:788–98. https://doi.org/10.1115/1.1900149.

[32] Hull R. Properties of Crystalline Silicontle. London : INSPEC, the Institution of Electrical Engineers; n.d.

[33] Guelpa V, Sandoz P, Vergara MA, Clévy C, Le Fort-Piat N, Laurent LGJ. 2D visual micro-position measurement based on intertwined twin-scale patterns. Sensors Actuators, A Phys 2016;248:272–80. https://doi.org/10.1016/j.sna.2016.08.002.

[34] Karl Pearson. Mathematical Contributions to the Theovy of Evolution.—III. Heredity, and Panmixia. Philos Trans R Soc London 1896;187:253–318. https://doi.org/10.1098/rsta.1896.0007.

[35] Huitson A, Dunn OJ, Clark VA. Applied Statistics: Analysis of Variance and Regression. vol. 25.

New York: Wiley; 1976. https://doi.org/10.2307/2987845.

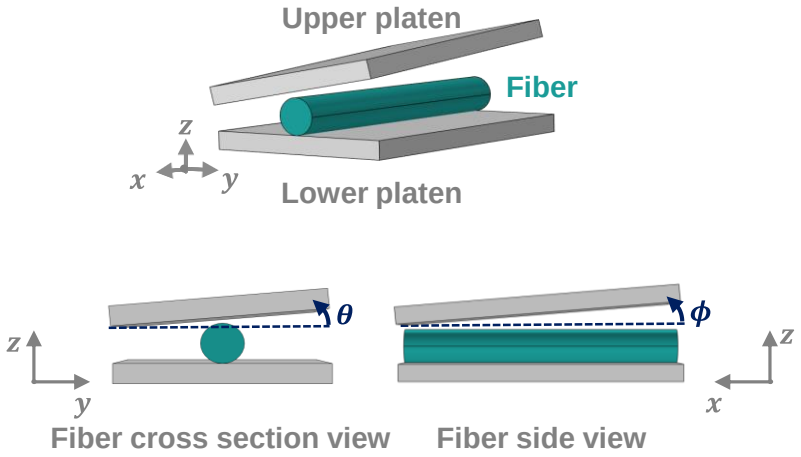

Fig. 1. Representation of the possible angles of an upper compression platen in SFCT. The angle ϕ is defined 'as tilt angle'.

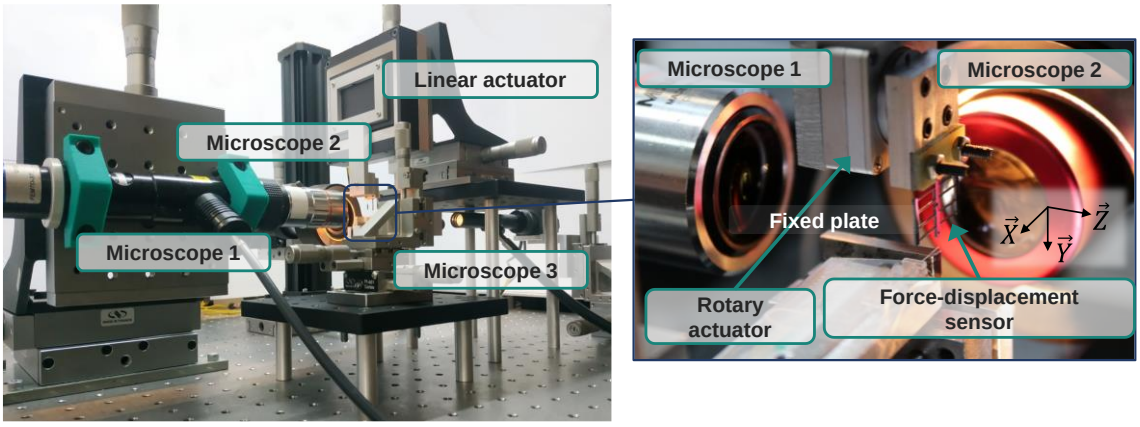

Fig. 2.Micro-mechatronic setup for SFTCT including: a linear actuator, a rotatory actuator, 3 microscopes and a force-displacement sensor. Numerous manual XYZ stages can be seen, for the positioning of each component.

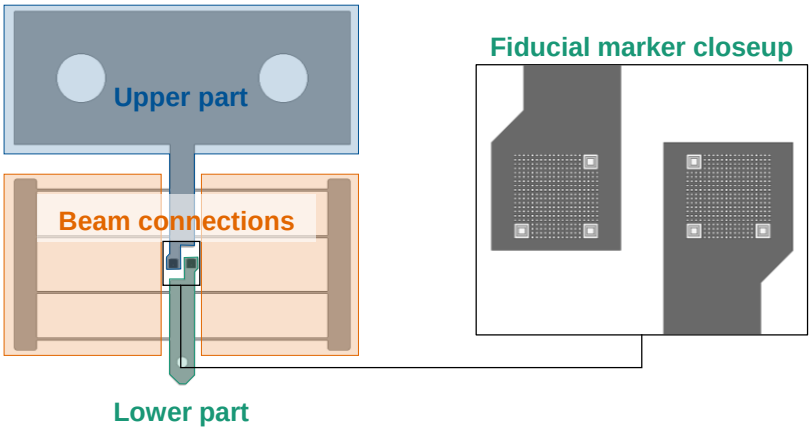

Fig. 3. Force-displacement sensor design with closeup view on fiducial markers.

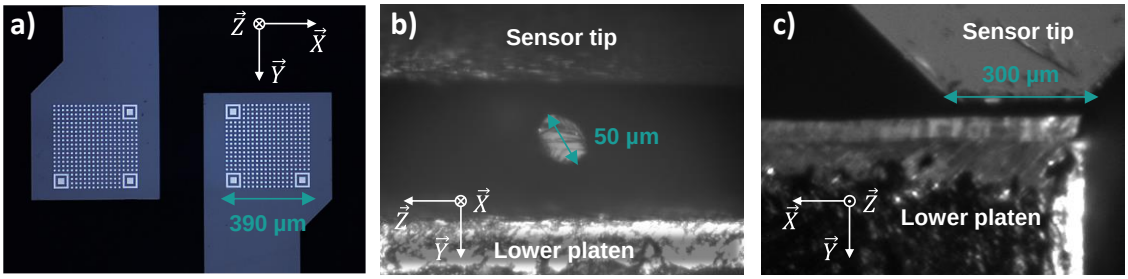

Fig. 4.Views from the 3 microscopes on the SFTCT setup: a) Force-displacement sensor fiducial marker view, b) Cross section view of PA11 fiber, c) Side view of PA11 fiber.

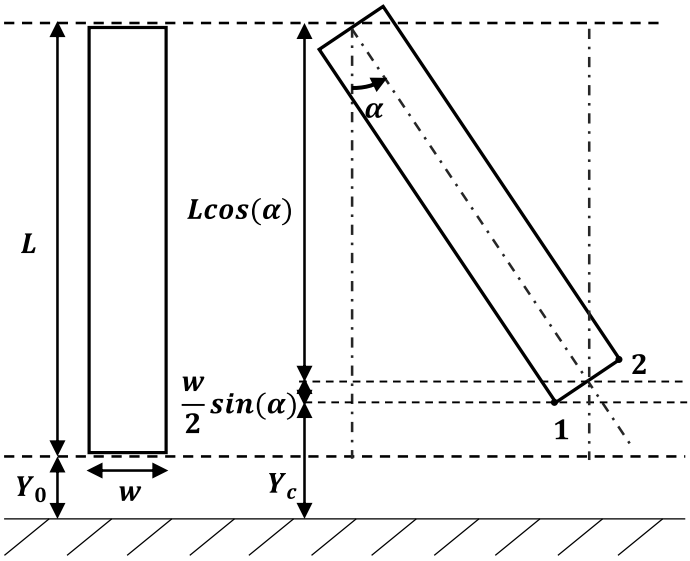

Fig. 5. Sensor- fixed bottom platen representation in a parallel state and with an angle α.

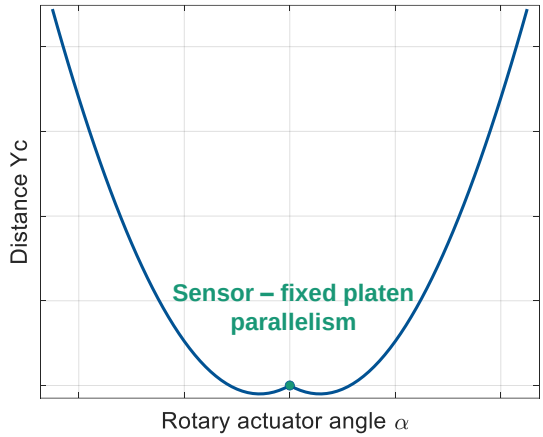

Fig. 6. Distance between sensor and fixed platen (Y_c) as a function of the angle given by the rotary actuator (α). The parallelism between the object is ensured for the angle at the tip of the ω shape.

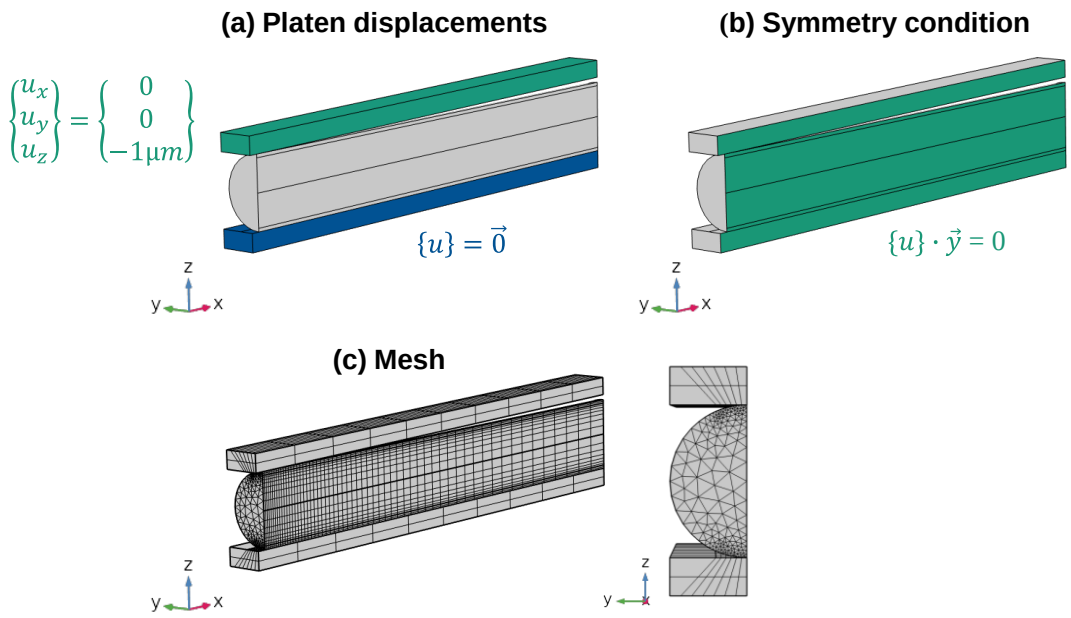

Fig. 7. Finite element model of SFTCT, including boundary conditions and mesh.

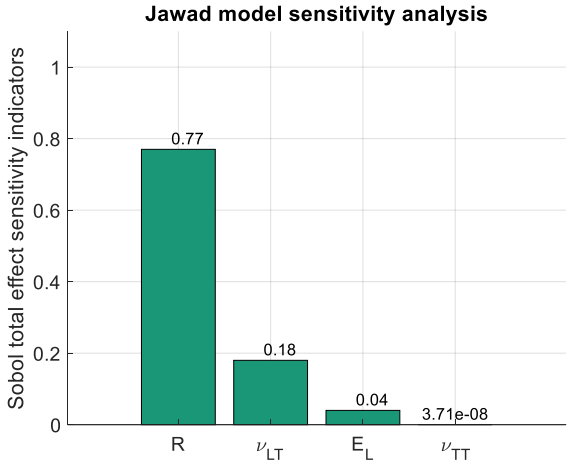

Fig. 8. Results of the E_T sensitivity analysis in Jawad's model.

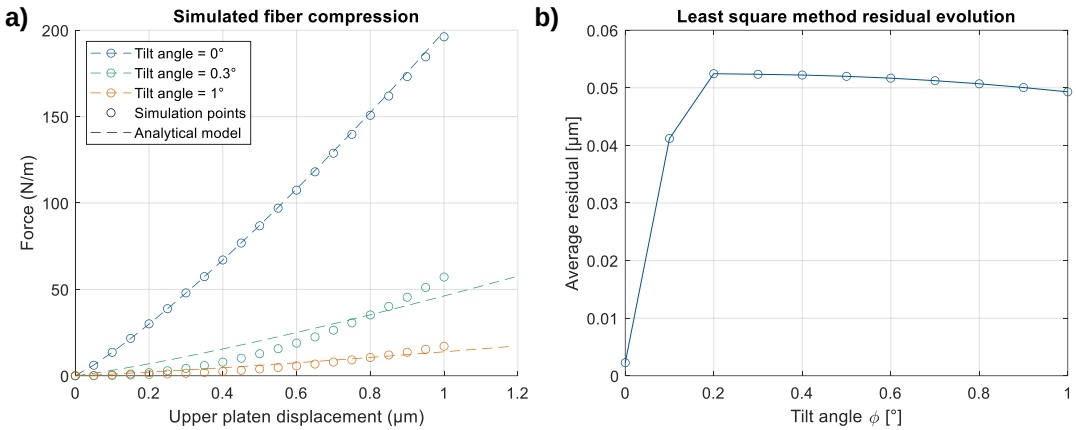

Fig. 9. Finite element tilt study results: a) compression force as a function of upper platen displacement for three different tilt angles, b) evolution of the average residue of the least squares regression.

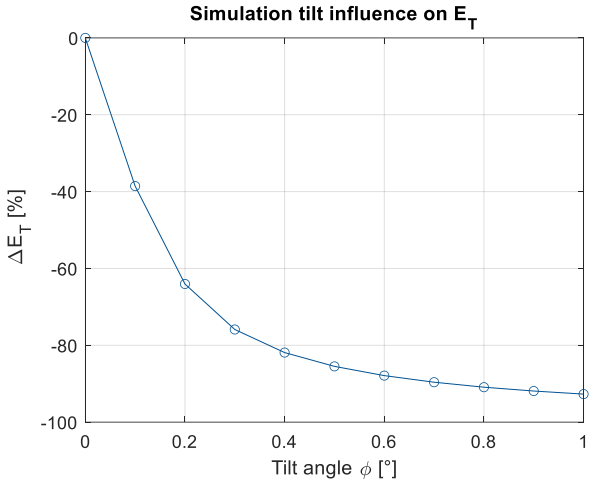

Fig. 10. Variation of the identified transverse elastic modulus as a function of the tilt angle in the case of the numerical tilt study.

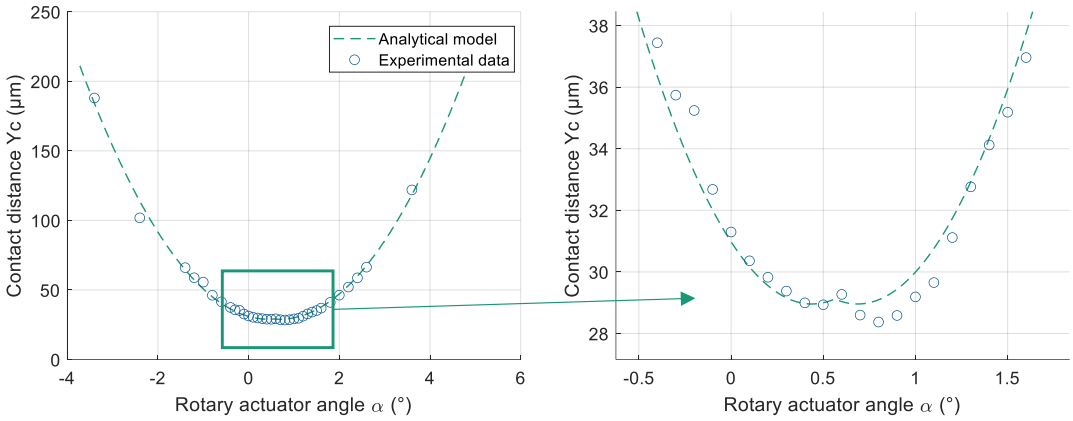

Fig. 11. Distance between sensor tip and fixed platen as a function of the angle of the rotary actuator. Fitting the analytical model to the experimental data gives the necessary rotation to minimize the tilt angle. The tilt is thus found at its minimum (ϕ=0°) when the actuator is rotated at $\alpha = 0.57°$ from its reference position.

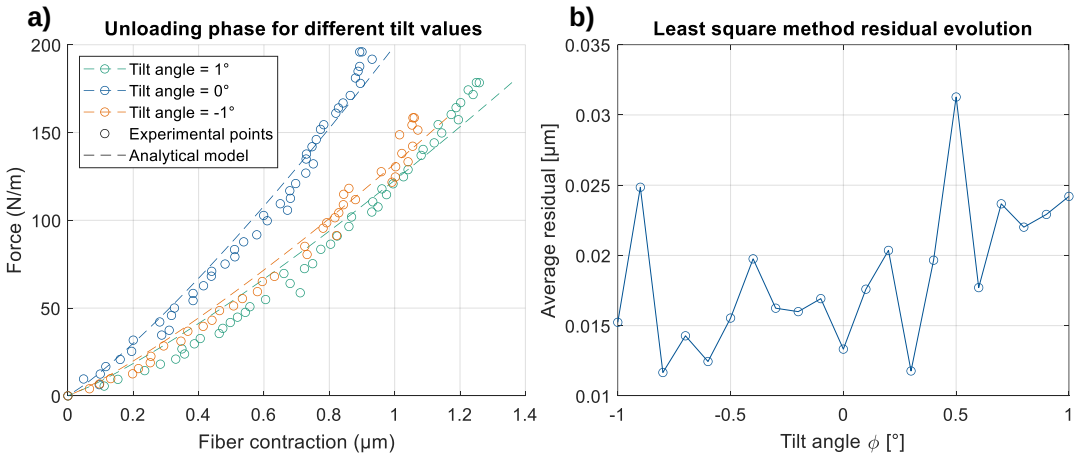

Fig. 12. Experimental tilt study results: a) compression force as a function of fiber contraction for three different tilt angles, b) evolution of the average residue of the least squares regression.

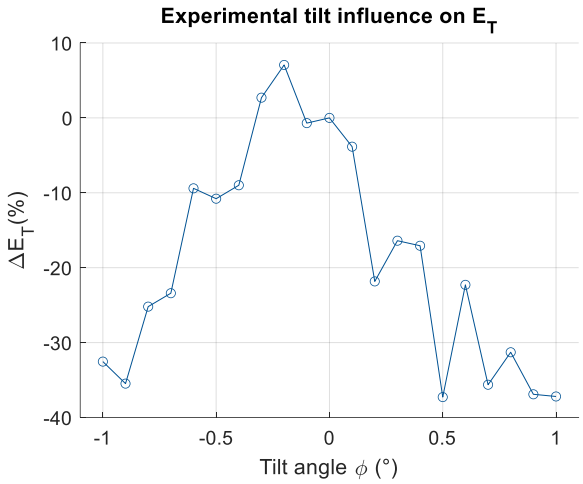

Fig. 13. Variation of the identified apparent transverse elastic modulus as a function of the tilt angle in the case of the experimental tilt study.

TABLE I PA11 fiber geometric and material parameters..

Parameter	Value	Source
$R(\mu m)$	17.05	FDAS measurement of PA11 fiber radius
$E_L(MPa)$	2155	Given by Placet et al. [30] for PA11 fiber
ν_{LT}	0.4	Given by Placet et al. [30] for PA11 fiber
ν_{TT}	0.07	Given by Placet et al. [30] for PA11 fiber
$E_T(MPa)$	706	Experimental measurements with parallel platens on PA11 fiber
Length(μm)	300	Compressed fiber length equal to sensor tip width

TABLE II Compression platen geometric and material parameters used in finite element simulation.

Parameter	**Value**	**Source**
Length(μm)	300	Equal to sensor tip width
Width(μm)	17.05	Equal to fiber radius
Young's modulus(GPa)	100	Chosen as significantly stiffer than the fiber and in the order of magnitude of silicon and aluminum